Optimal and Robust Design of the Laser Forming Process

Chao Liu and **Y. Lawrence Yao,** Dept. of Mechanical Engineering, Columbia University, New York, New York, USA

Abstract

The laser forming process of sheet metal has been extensively analyzed, but few attempts have been made in the area of process design. The task of the process design in the laser forming of sheet metal is to determine a set of parameters, including laser scanning paths, laser power, and scanning speed, given a prescribed shape. Response surface methodology is used as an optimization tool. The propagation of error technique is built into the design process as an additional response to be optimized via desirability function and hence make the design robust. Focusing on a class of shapes, the design scheme is applied progressively in four cases in which issues such as a large number of design variables are properly addressed.

Keywords: Optimal Design, Response Surface Methodology, Propagation of Error, Laser Forming

1. Introduction

Compared with conventional forming techniques, laser forming of sheet metal does not require hard tooling or external forces and, hence, can increase process flexibility and reduce the cost of the forming process when low to medium production volume is concerned. Many efforts have been made on mechanisms and modeling of the process. Magee, Watkins, and Steen (1998) reviewed literature available up to 1998. More recently, selected issues related to extending laser forming to more practical applications have started being addressed. For instance, repeated scanning is necessary to obtain the magnitude of deformation that practical parts require, and hence cooling effects during and between consecutive scans become critical (Cheng and Yao 2001a). Another example is to consider the dependence of material flow stress on the microstructure change in modeling laser forming with repeated scanning, where material undergoes heating and cooling cycles (Cheng and Yao 2001b).

A vast majority of work on laser forming, including that mentioned above, can be considered as solving the direct problem, that is, finding the spatial and temporal distribution of temperature, strain/stress state, and ultimately, deformation of a workpiece, given process and material parameters. Such a problem is typically formulated based on physical laws such as heat transfer and elasticity/plasticity theories. The solution to such a problem may take an analytic form such as the well-known solution to a moving heat source problem that includes a Bessel function, or require a numerical method such as the finite element method (FEM) for plate/shell deformation. More specifically, the following mapping *F* can be analytically or numerically found:

$$U = F(\Theta, \Phi, \Gamma, t) \qquad (1)$$

where *U* represents deformation of the given workpiece, Θ process parameters, including laser power, beam scanning velocity, beam diameter, and laser paths, Φ material properties, Γ coordinates, and *t* time.

To apply the laser forming process to real-world problems, however, the inverse problem needs to be addressed, that is, to design process parameters Θ given a desired shape *U*. More specifically, the inverse problem is to find mapping *g*.

$$\Theta = g(U, \Phi, \Gamma, t) \qquad (2)$$

Solving the inverse problem analytically or numerically is difficult, if not impossible, for the following reasons. First, Eq. (1) is obtained by solving differential equations based on physical laws, while no physical laws are readily available to establish governing equations leading to the solution shown in Eq. (2). Second, to manipulate either the solution to the direct problem [Eq. (1)] or the underlying differential equations leading to a solution to the inverse problem is also impossible because of the complexity involved or because parts such as the
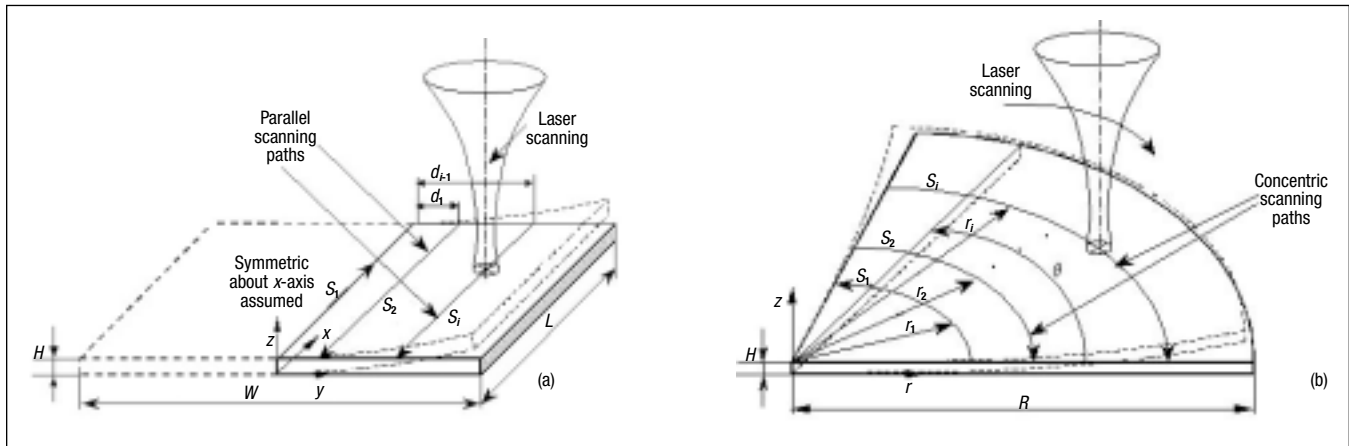
Figure 1
Schematic of a Class of Shapes To Be Laser Formed
(a) Linear parallel scanning paths on a rectangular plate and (b) Concentric paths on a quarter-circle plate (θ represents in-plane angle)

Bessel function mentioned above do not lend themselves to manipulation (Vollertsen 1994). Third, while the solution to the direct problem is unique, the solution to the inverse problem is certainly multi-valued. There could be more than one Θ for the same desirable shape U.

Given the understanding that numerical or analytical solutions to the inverse problem are less likely, empirical and heuristic approaches have been attempted. Hennige (2000) and Magee, Watkins, and Hennige (1999) investigated the irradiation patterns for a type of axis-symmetric shapes—spherical shapes. Based on prior knowledge of the laser forming process, radial and concentric irradiation paths were postulated and tested. Advantages and disadvantages of each, as well as their various combinations, were shown and compared. Other process parameters were only dealt with marginally. A genetic algorithm (GA) based approach, which is an adaptive heuristic search algorithm premised on the evolutionary ideas of natural selection and genetics, was proposed by Shimizu (1997) as an optimization engine to solve the inverse problem of the laser forming process. In his study, a set of arbitrarily chosen heat process conditions for a dome shape was encoded into strings of binary bits, which evolve over generations following the natural selection scheme. One of the important process parameters, heating path positions, was assumed given. To apply GA, it is necessary to specify crossover rate and mutation rate, but their selection suffers from lack of rigorous criteria.

The objective of this paper is to develop a more systematic and reliable methodology to solve the inverse problem in laser forming for a class of shapes. A response surface methodology (RSM) based approach is attempted as an optimization tool. Discrete design variables are properly dealt with in the optimization process. The propagation of error (POE) technique is built into the design process as an additional response to be optimized via a desirability function and hence make the design more robust. Experiments and, at places, the finite element method (FEM) are used to enable and validate the optimization process. The proposed approach is applied to four cases, which are progressively more involved, to demonstrate its validity.

2. Problem Description

As shown in *Figure 1*, rectangular or circular sheet metal is to be formed into 3-D shapes by parallel or concentric laser irradiation paths S_1, S_2, ..., and S_N. If the variation of laser-induced bending angle along a particular irradiation path is not considered, that is, the edge effects in the laser forming process are neglected (Bao and Yao 2001), the 3-D shapes can be viewed as shapes generated by a 2-D generatrix in the y-z plane extruded in the x direction for the rectangular case (*Figure 1a*), and by a 2-D generatrix in the r-z plane revolved around the z axis for the circular plate case (*Figure 1b*). Therefore, for this class of 3-D shapes, the inverse design problem can be treated as a 2-D curve design problem. The 2-D curve is the generatrix, which is assumed given in the inverse problem.

As shown in *Figure 1*, the parameters needed to be determined include number of scanning paths, N; positions of laser scanning paths, d_i ($i = 1, 2, ..., N-1$) for the rectangular case or r_i ($i = 1, 2, ..., N-1$) for the circular case; laser powers, p_i ($i = 1, 2, ..., N$); beam scanning velocity, v_i ($i = 1, 2, ..., N$); and laser spot diameter, D_b. Among them, d_i and r_i should remain within the plate; that is, $d_i \leq \frac{W}{2}$, and $r_i \leq R$, where W is the width of the rectangular plate and R is the radius of the circular plate. Assuming a constant laser spot diameter, D_b, for all the paths implies the 2-D generatrix curve being monotonic for simplicity without loss of generality. The approach presented in this paper, however, is not restricted to monotonic cases. A nonmonotonic generatrix (i.e., combination of convex and concave sections) can be similarly dealt with using different beam spot sizes for different paths. As is well known, a smaller spot size compared with sheet thickness favors the temperature gradient mechanism leading to concave bending, while a larger spot size favors the buckling mechanism likely leading to convex bending. In a real-world problem, not all the parameters mentioned above need to be determined in the design process; some of them are required to be kept constant.

In the optimal design process based on the response surface methodology presented in this paper, the objective is to minimize the difference between a possible solution shape and the prescribed shape, that is

$$\text{Minimize } h = \sqrt{\frac{\sum_{i=1}^{k}\left(z_{si} - z_{pi}\right)^2}{k}} \qquad (3)$$

where z_s and z_p are the z coordinates of corresponding points on the generatrix of the possible solution shape and the prescribed shape, respectively, and k is the number of points. It will be seen that values of the objective function h in fact serve as responses in the optimization process. In addition, if a point in the possible solution shape has a smaller z value than the corresponding point of the prescribed shape, the distance is defined as negative; otherwise, it is positive. When the sum of the distances is positive, the objective (or response) is considered positive; otherwise, it is negative. That is, $sign\left(\sum_{i=1}^{k}\left(z_{si} - z_{pi}\right)\right)$ determines the sign of the
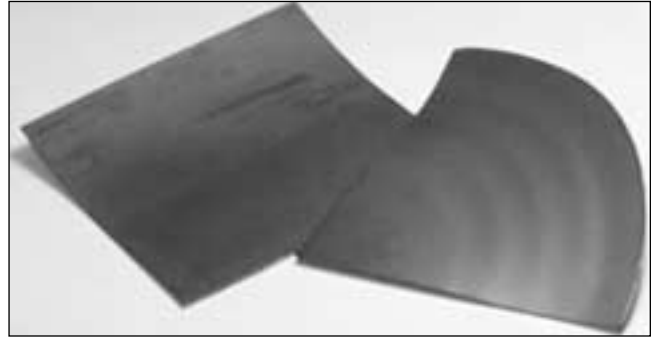

Figure 2
Typical Laser-Formed Samples Using Scanning Schemes Shown in *Figure 1*

objective (or response). It is necessary to consider the sign in order to determine if more or less deformation is needed.

The final design of a product is required not only to be optimal but also robust, namely, insensitive to the variation of input variables. In the laser forming process, the achievable accuracy of forming is limited by numerous uncertainties. Hennige, Holzer, and Vollertsen (1997) investigated influencing uncertainties in laser forming based on analyzing error propagation. They found that variations in power and the coupling coefficient are the most influential factors on the variation of deformation. In this paper, the influence of laser power on the robustness of the optimal design will be addressed in a robust design phase based on desirability consideration.

In this study, square plates of size 80×80×0.89 mm and quarter-circle plates of 80 mm radius and 0.89 mm thickness are used. For the circular plate, the in-plane angle θ is defined as the angle between the front cross-section plane and a cross-sectional plane perpendicular to the concentric scanning paths (*Figure 1b*). The material used is AISI1012 low-carbon steel. The laser system used is a 1500W CO_2 laser. In all the experiments, the laser beam diameter is set to 4 mm and beam moving velocity is kept constant at 50 mm/s. To enhance laser absorption by the workpiece, graphite coating is applied to the irradiated surface. Typical samples of formed plates are shown in *Figure 2*. A coordinate measuring machine (CMM) is used to measure the coordinates of the deformed plates.

3. Response Surface Methodology and Optimal Design

Response surface methodology (RSM) is a collection of statistical and mathematical techniques

useful for developing, improving, and optimizing process (Myers and Montgomery 1995). Applications of RSM comprise two phases. In the first phase, the response surface function is based on a factorial design, approximated by a first-order regression model [Eq. (4)], and complete with steepest ascent/descent search, until it shows significant lack of fit with experiment data, or until there is no direction of improved response. After reaching the vicinity of the optimum, the second phase of the response surface function is approximated by a higher order regression function such as a second-order one shown in Eq. (5).

$$\hat{y} = b_0 + \underline{b_1}^T \underline{x} + \varepsilon \qquad (4)$$

$$\hat{y} = b_0 + \underline{b_1}^T \underline{x} + \underline{x}^T \underline{\underline{b_2}}\, \underline{x} + \varepsilon \qquad (5)$$

where $\hat{y}$ and $\underline{x} = [x_1, x_2, \ldots, x_n]^T$ are estimated response and decision variable vectors, respectively, ε is a fitting error that is assumed to be normally distributed, and b_0, $\underline{b_1} = [b_{11}, b_{12}, \ldots, b_{1n}]^T$, and

$$\underline{\underline{b_2}} = \begin{bmatrix} b_{211} & b_{212} & \cdots & b_{21n} \\ b_{221} & & & \\ \cdots & & & \\ b_{2n1} & \cdots & \cdots & b_{2nn} \end{bmatrix}$$

are coefficient scalar/vector/matrices determined using the least-square regression. The model in Eq. (5) is then differentiated with respect to the decision variables to determine the optimum condition for the forming process. As mentioned earlier, among the design variables to be determined, the number of laser scans, N, is an integer variable, which is not appropriate for Eq. (5) and thus the branch-and-bound method is employed (Taha 1987).

Suppose among n decision variables, q of them are integers. The general idea of the method is to first solve the problem as a continuous model, and then generate a sequence of subproblems. The process is repeated until each of the subproblems can be easily solved.

The steepest line search starts with the initial design points of q integer variables and $n - q$ non-integer variables. The next iteration starts by arbitrarily choosing a design point from one of the q integer variables. The remaining $q - 1$ design points of integer variables of the next movement are determined based on the coefficient from Eq. (4) and the branch-and-bound method. After reaching the vicinity of optimum, the response surface is approximated by a higher regression order with q integers determined from previous iterations and $n - q$ non-integer factors. At this stage, the problem can be solved as a regular one with $n - q$ continuous variables.

4. Desirability and Robust Design

Optimization design may not accomplish the desired result due to the influence of uncontrollable noise and variation of the input factors. Therefore, designs are sought that are not only optimal but also robust (insensitive) to inevitable changes in the noise and input factors. Robust design methods represent a systematic approach for finding the near-optimum combination of design parameters, and yet the design is insensitive to variation in both controllable input variables and/or uncontrollable noise factors. Taguchi introduced parameter designs with inner and outer arrays and signal-to-noise ratio as robust optimization criterion to identify factor settings that minimize variation in performance (Myers and Montgomery 1995). However, these designs tend to have a large number of runs and become inefficient relative to the amount of information they provide. In the laser forming process, the achievable accuracy of the bending angle is a result of many different parameters. Hennige, Holzer, and Vollertsen (1997) analyzed the effect of variations in various variables on deformation in laser forming using the well-known error propagation equation and gave a very good sense as to the relative influence of these variations on deformation variation. But the analysis made no connection with process design.

Desirability-based robust design is a tool to find controllable factor settings that optimize the objective yet minimize the response variation of the design (Kraber and Whitcomb 1996, Derringer and Suich 1980). It requires construction of a response surface using a mathematical model [Eq. (5)]. The transmitted variation of responses from input variables can thus be reduced by moving the optimal solution to a flatter part of the response surface. The variation transmitted to the response can be determined by the well-known error propagation equation, which is modeled by taking the partial derivatives of the polynomial [Eq. (5)] with respect to the decision variables.

$$POE = \hat{\sigma}_y = \left(\sum_{i=1}^{n} \left(\frac{\partial \hat{y}}{\partial x_i} \right)^2 \sigma_{ii}^2 + \sum_{i<j}^{n} 2 \frac{\partial \hat{y}}{\partial x_i} \frac{\partial \hat{y}}{\partial x_j} \sigma_{ij}^2 + \sigma_e^2 \right)^{1/2} \qquad (6)$$

where $\hat{\sigma}_y$ is the model-predicted standard deviation of the response, or known as propagation of error (POE), σ_{ii}^2 is the variance of decision variable x_i, σ_{ij}^2 is the covariance between x_i and x_j, σ_e^2 is the residual variance, $\sigma_e^2 = \dfrac{\sum_{j=1}^{} \varepsilon_j^2}{df}$, and *df* is the residual degree of afreedom, which equals the number of response values *k* minus the number of terms in the regression model. To reduce variance in the response, POE [Eq. (6)] should be minimized; therefore, it can be treated as an additional response built into the design process. The simultaneous optimization of several responses [in this case, *y* in Eq. (5) and $\hat{\sigma}_y$ in Eq. (6)] is the essence of the desirability-based robust design (Kraber and Whitcomb 1996, Derringer and Suich 1980).

For each response $\hat{y}_i$, a desirability function $D_i(\hat{y}_i)$ assigns a value between 0 and 1 to the possible values of $\hat{y}_i$, with $D_i(\hat{y}_i)$ representing a completely undesirable value of $\hat{y}_i$ and $D_i(\hat{y}_i)$ representing the ideal response value. The individual desirabilities are then combined using the geometric mean, which gives the overall desirability *D*

$$D = \left(D_1(\hat{y}_1) \times D_2(\hat{y}_2) \times \ldots \times D_m(\hat{y}_m) \right)^{1/m} \qquad (7)$$

where *m* is the number of responses. The maximum of *D* represents the highest combined desirability of the responses. Depending on whether a particular response $\hat{y}_i$ is to be maximized, minimized, or assigned to a target value, different desirability functions $D_i(\hat{y}_i)$ are to be used.

Let L_i, U_i, and T_i be the lower, upper, and target values desired for response $\hat{y}_i$, respectively, where $L_i \leq T_i \leq U_i$. If a response is of the "target is best," its desirability function is expressed as:

$$D_i(\hat{y}_i) = \begin{cases} 0 & \text{if } \hat{y}_i < L_i \\ \left[\dfrac{\hat{y}_i - L_i}{T_i - L_i} \right]^r & \text{if } L_i \leq \hat{y}_i \leq T_i \\ \left[\dfrac{\hat{y}_i - U_i}{T_i - U_i} \right]^s & \text{if } T_i \leq \hat{y}_i \leq U_i \\ 0 & \text{if } \hat{y}_i > U_i \end{cases} \qquad (8)$$

where the exponents *r* and *s* determine how strictly the target value is desired. If a response is to be minimized, the individual desirability is instead defined as

$$D_i(\hat{y}_i) = \begin{cases} 1 & \text{if } \hat{y}_i < T_i \\ \left[\dfrac{\hat{y}_i - U_i}{T_i - U_i} \right]^s & \text{if } T_i \leq \hat{y}_i \leq U_i \\ 0 & \text{if } \hat{y}_i > U_i \end{cases} \qquad (9)$$

where *T* represents a small enough value for the response.

Maximization of $\hat{y}_i$ is equivalent to minimization of $-\hat{y}_i$. As seen from Eqs. (5) and (6), $\hat{y}_i$ is a continuous function of x_i; it follows that D_i and *D* are piecewise, continuous functions of x_i. The above numerical optimization problem reduces to a general nonlinear problem with constraints. However, as seen from Eqs. (7) to (9), the derivative of *D* is not continuous. Therefore, direct search methods need to be applied to find the optimal value of *D*. The downhill simplex method (Miller 2000) requires only function evaluations and is chosen in this study. In an *n*-dimensional search space, it starts with an initial simplex of *n*+1 vertices. It requires a comparison of the objective function values at a limited number of search points, specifically *n*+1 points, in the *n*-dimension search space. An implementation of the algorithm is Design-Expert® by Stat-Ease, Inc, which is used in the paper.

5. Approach to Bending Angle Attainment

In the steepest ascent/descent search and RSM process, a large number of experiments are required to obtain bending angles under different conditions, which is time consuming and costly and thus poses a serious limitation to the method. If the total deformation of a sheet generated by the parallel or concentric laser scans can be obtained by summing deformations generated by these scans, a much smaller number of experiments will suffice. In other words, if deformations caused by scans at different d_i or r_i (*Figure 1*) can be considered independent of each other, only experiments with single scanning paths are needed. This hypothesis is supported by FEM (to be explained in the subsequent section) results shown in *Figure 3*, in which it is illustrated that for a laser beam spot size of 4 mm, typical temperature and compressive plastic strain rise is
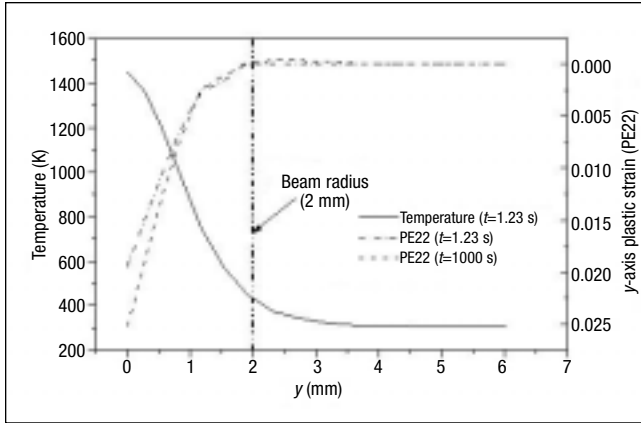
Figure 3
**Simulation Results Showing that Temperature and Compressive
Plastic Strain Rise Do Not Go Beyond the Extent of Laser Beam Size
(square plate, scanning path at *y*=0 mm, *p*=650 W, and
beam spot size = 4 mm)**

largely confined within the beam spot size. The effect of temperature and plastic strain is negligible outside the region. Therefore, when the spacing between two adjacent irradiation paths $d_i - d_{i-1}$ (or $r_i - r_{i-1}$) is sufficiently large, the development of the bending angle can be assumed independent of one another. Consequently, experimental results of single scans are shown in *Figure 4*. The hypothesis of independence will be further tested in the result and discussion section.

Figure 4a, adapted from Cheng and Yao (2001a), is for the square plate under different laser power levels at a scanning velocity of 50 mm/s. The scanning was done at $y = 0$ and the bending angle is assumed to be the same if scanning is done at a non-zero y value. This is appropriate because the plate size is relatively small. Hsiao et al. (1997) reported that the amount of angular distortion is sensitive to the physical size of the specimen, if the size is large. A line is fitted through the data points to allow interpolation in between. *Figure 4b* shows single concentric scan experimental results of the circular plate at different radial positions and power levels. As seen, the bending angle varies with the radial position of the laser concentric scanning path, r_i. This is not the case for the square plate, as explained above. This variation will be explained shortly using *Figure 5*. FEM results are also superposed in *Figure 4b* and reasonable agreements are seen. The results in *Figure 4b* are also fitted with a surface as shown in *Figure 4c* to allow interpolation in between. Because of the nonlinear and nonmonotonic nature as shown in *Figure 4b*, a third-order least-square surface is employed as seen in *Figure 4c*.
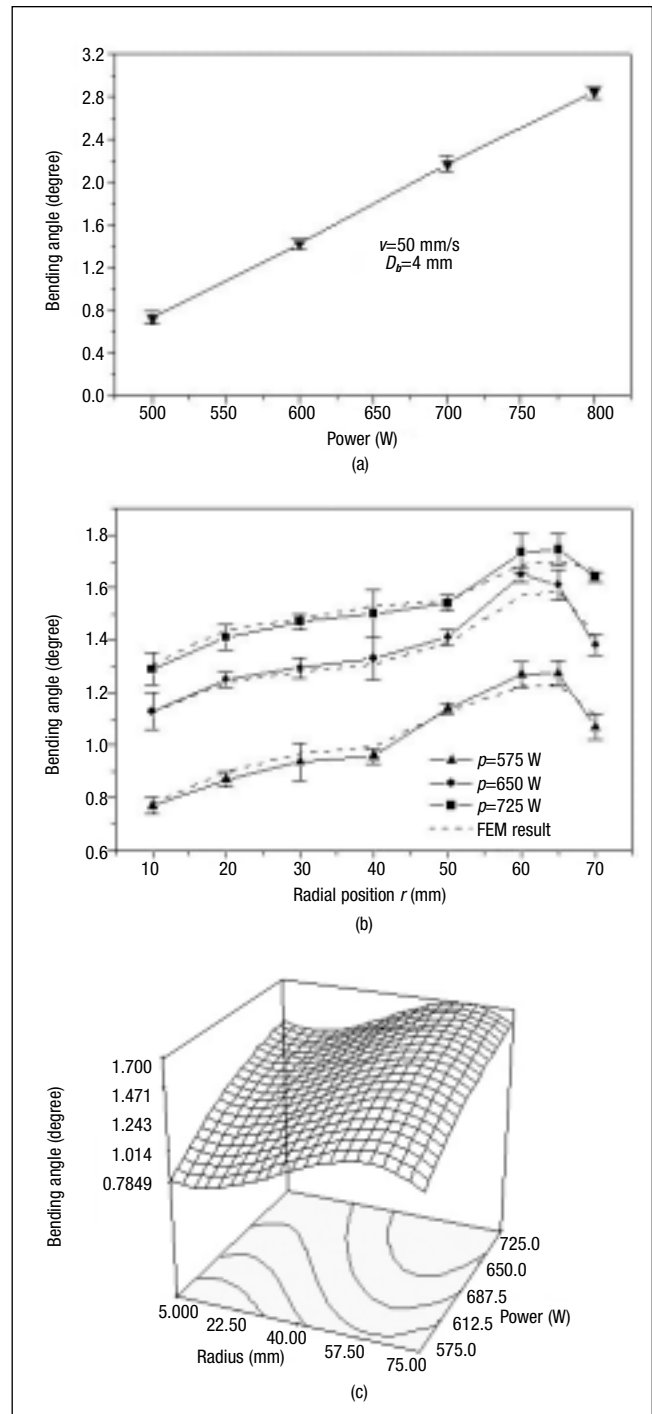
Figure 4
**Bending Angle Induced by a Single Scan
(a) Experimental results of square plate (Cheng and Yao 2001a); (b)
Experimental and simulation results of quarter-circle plate; and (c) a
third-order fitted surface based on data shown in *Figure 4b***

Figure 4b shows an interesting pattern in which the bending angle first increases with the radial position of laser concentric scanning path, r_i, and then falls when the scanning path is near the outer edge of the quarter circle plate for a given laser
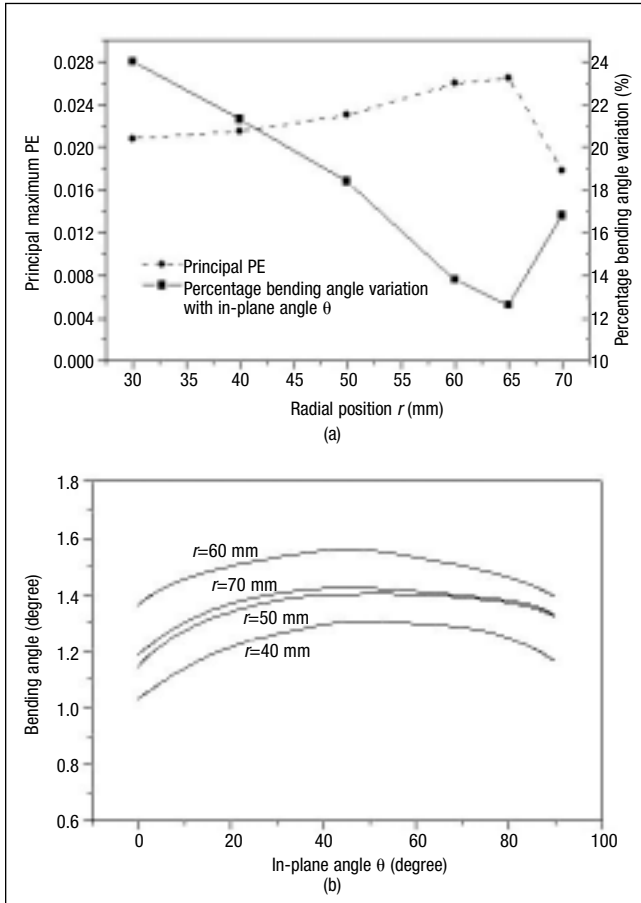
Figure 5
Simulation Results of Quarter-Circle Plate
(a) Principal plastic strain and percentage bending angle variation along laser scanning path and (b) Bending angle variation along concentric laser path (p=650 W)

power level. At about r = 65 mm, the angle is the largest. A larger bending angle is indicative of smaller geometric constraint because the laser power is kept the same for scans at different radii. To help explain the phenomenon, corresponding FEM results are plotted in *Figure 5*. As seen in *Figure 5a*, the maximum principal plastic strain on the scanning path (shown in dotted lines), which is proportional to the deformation at the location, first increases until about r = 65 mm and then decreases. It shows a similar pattern as the bending angle but does not explain the pattern. *Figure 5b* shows the bending angle variations with the in-plane angle θ at different radial positions. The variation is caused by, among others, geometric constraints imposed especially by both edges (ends) of the scanning path, which have been extensively dealt with previously (Bao and Yao 2001). The percentage of bending angle variation with in-plane angle θ, which is defined as (max-min)/max, are superimposed in

Figure 5a in solid lines. It is seen that the percentage of bending angle variation decreases with the radial position of the laser concentric scanning path, r_i, to about 65 mm and then increases. The larger the variation is, the larger the geometric constraints, and thus the smaller the bending angle. When the radius of the scanning path, r_i, increases, the length of the scanning path increases. As a result, the relative geometric constraints decrease and thus the bending angle increases until about r = 65 mm. When the position of the scanning path moves further outward, the bending angle decreases. This is because additional geometric constraints are brought about by the encroached outer edge of the workpiece.

6. Numerical Simulation

As seen in the preceding section, the FEM results play a useful role in helping test hypotheses (*Figure 3*), ascertaining experimental results (*Figure 4b*), and helping explain observed phenomena (*Figure 5*). In this section, governing relations underlying the FEM results are briefly outlined.

The following assumptions are made. The workpiece material is isotropic. Material properties such as Young's modulus, yield stress, heat transfer properties, thermal conductivity and specific heat, are temperature dependent. The heat flux F_L of the laser beam follows Gaussian distribution. No melting is involved and no external forces are applied in the forming process.

The temperature distribution of the workpiece can be obtained by solving the heat conduction equation. The associated boundary conditions of the heat conduction equation are: $z = H$: $\alpha_{abs}F_L \cdot \hat{n} = -\hat{n} \cdot (K\nabla T)$ (*Figure 1*), where α_{abs} is the material's absorbency and $\hat{n}$ is the unit vector normal to the surface pointing to the solid. All the surfaces are subject to natural heat convection and radiation.

Because no external forces exert on the faces of the workpiece ($z = 0$ and H), the traction-free boundary condition is assumed, namely $\sigma_{ij} \cdot \hat{n} = 0$. The elastic strain can be expressed as

$$\varepsilon_{ij}^e = \frac{1}{2}\left(\frac{\partial u_i}{\partial x_j} + \frac{\partial u_j}{\partial x_i}\right)$$ where u is the displacement

function. When Von Mises criterion is applied to the plastic potential function, the flow rule can be

Figure 6
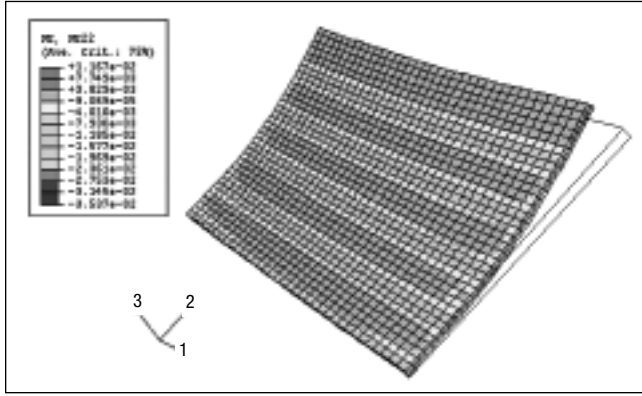**Typical FEM Result of Parallel Scanning of Square Plate 80×80×0.89 mm (half is shown due to symmetry). PE22 is plastic strain in *yy* direction (*p*=650 W, *t*=1.8 s, beam moving velocity is 50 mm/s, five scan paths).**

expressed as $\dfrac{d\varepsilon_1}{s_1} = \dfrac{d\varepsilon_2}{s_2} = \dfrac{d\varepsilon_3}{s_3} = d\lambda$, where s_1, s_2, and s_3 are principal components of the deviatoric stress tensor (Kobayashi 1989). With the introduction of effective stress and effective strain rate, $\dot{\lambda}$ can be expressed as $\dot{\lambda} = \dfrac{3}{2}\dfrac{\dot{\bar{\varepsilon}}}{\bar{\sigma}}$, where

$\bar{\sigma} = \sqrt{\dfrac{3}{2}\left(s_{ij}s_{ij}\right)}$ and $\dot{\bar{\varepsilon}} = \sqrt{\dfrac{2}{3}\left(\dot{\varepsilon}_{ij}\dot{\varepsilon}_{ij}\right)}$ are effective stress and effective strain rate, respectively. The relationship between deviatoric stress and plastic strain rate therefore can be written as:

$$\dot{e}_{ij}^{p} = 0 \qquad \text{if } \frac{1}{2}s_{ij} < \kappa^2(T), \text{ or if } \frac{1}{2}s_{ij} = \kappa^2(T)$$
$$\text{and } s_{ij}\dot{s}_{ij} - 2\kappa\kappa' T \leq 0$$

$$\dot{e}_{ij}^{p} = \dot{\lambda}s_{ij} \quad \text{if } \frac{1}{2}s_{ij} = \kappa^2(T) \qquad (10)$$
$$\text{and } s_{ij}\dot{s}_{ij} - 2\kappa\kappa' T \geq 0$$

By combining the elastic strain rate, plastic strain rate, and thermal strain rate components, the total strain rate can be expressed as (Boley and Weiner 1997):

$$\dot{e}_{ij} = s_{ij}\dot{\lambda} + \frac{1}{2G}\dot{s}_{ij} +$$
$$\delta_{ij}\left(\frac{1-2\upsilon}{E}\right)\dot{\sigma} + \delta_{ij}\alpha\dot{T} \qquad (11)$$

where G is shear modulus and υ is Poisson's ratio.

In the square plate simulation, symmetry about the *x*-axis is assumed; only half of the plate is simulated. The symmetric plane is assumed to be adiabatic. Two adjacent points in the middle of the symmetric plane are fixed to remove the rigid body motion. All the nodes in the symmetric plane are removed of freedom in *y*-direction. In the quarter-circle plate simulation, three adjacent nodes near *r* = 0 are removed of freedom in all directions. The same mesh model is used for the heat transfer analysis and structural analysis. Commercial FEM software, ABAQUS, is used to solve the thermal mechanical problem. In the structural analysis, the 20-node element type, C3D20, has no shear locking, no hourglass effect, and is thus suitable for a bending-deformation-dominated process such as laser forming. To remain compatible with the structural analysis, the 20-node element type, DC3D20, is used in the heat transfer analysis. *Figure 6* shows a typical FEM result of five parallel scans at *p* = 650 W. The color contour represents the *y*-axis plastic strain distribution at time *t* = 1.8 seconds.

7. Results and Discussions

The independence hypothesis described in section 5 is experimentally and numerically tested. As discussed, the hypothesis states that the total deformation of the workpiece generated by multiple irradiation paths is the summation of deformations induced by the paths, provided the distance between adjacent paths is not too small. *Figure 7* shows that the hypothesis holds well under the conditions used. In *Figure 7a*, square plates are irradiated by equally spaced parallel laser paths, and the resultant deformations are measured using CMM and indicated in dots. On the same plot, bending angles of single scans obtained from *Figure 4a* are summed to determine the total deformation shown in solid lines. As seen, there is good agreement between the two. This is indicative of the validity of the independence hypothesis. In addition, note that the number of paths *N* ranges from 3, 5, 8, and 10, and therefore the independence holds at least for *N* = 10. For *N* = 10, the distance between adjacent paths is *W*/2/10 = 4 mm, and therefore both temperature rise and plastic strain at the adjacent paths don't overlap significantly (*Figure 3*). FEM results for *N* = 3 and 5 also show good agreements with experiments. Similar results are shown in *Figure 7b* for the quarter-circle plate, where four equally spaced concentric scannings were carried out at *r* = 40, 50, 60, and 70. The multiscanned plate is measured using CMM along
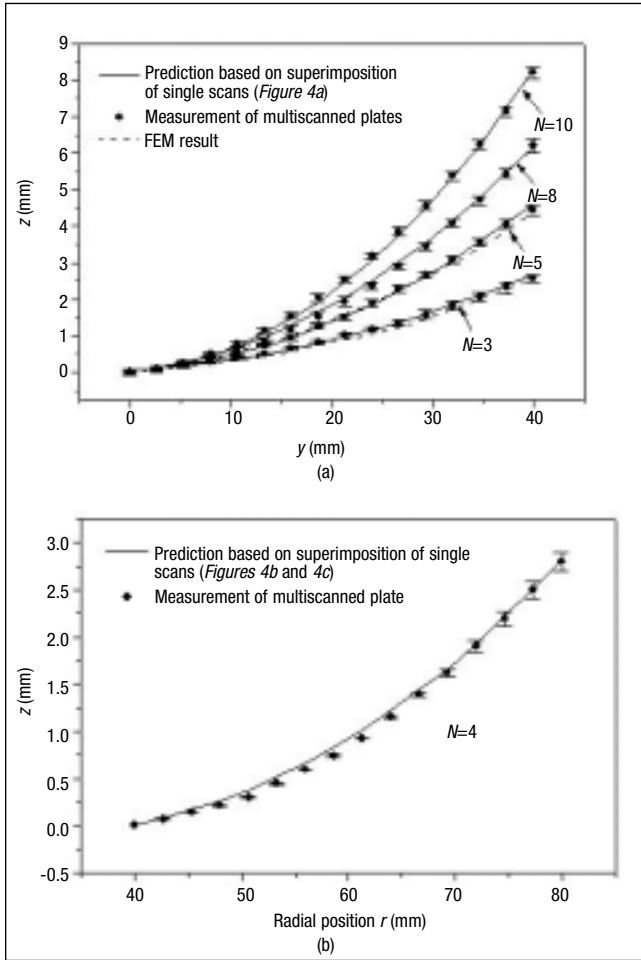
Figure 7
Comparison of Experimental Multiscanned Generatrix Shape with
Prediction Based on Superposition of Single Scans (a) Square plate,
FEM results based on single scans included and (b) Quarter-circle
plate (error bars represent standard deviation of two to four samples;
N is number of equally spaced scanning paths, *p*=650 W)

the in-plane angle $\theta = 45°$, and the measurement
result is shown in dots in the figure. On the same
figure, a line is drawn by summing the bending
angles of single scans at different radial positions
(*Figures 4b* and *4c*). The good agreement between
the two indicates that the concentric scans can be
considered independent each other at least down to
a distance of 10 mm for the case.

The optimal and robust design methodology out-
lined in this paper is applied in four inverse design
cases. The first two deal with the square plates with
parallel laser scanning paths, and the other two deal
with the quarter-circle plates with concentric laser
scanning paths. The integer design variable problem
is dealt with in Case 1. To reduce the number of
design variables, a control function approach is
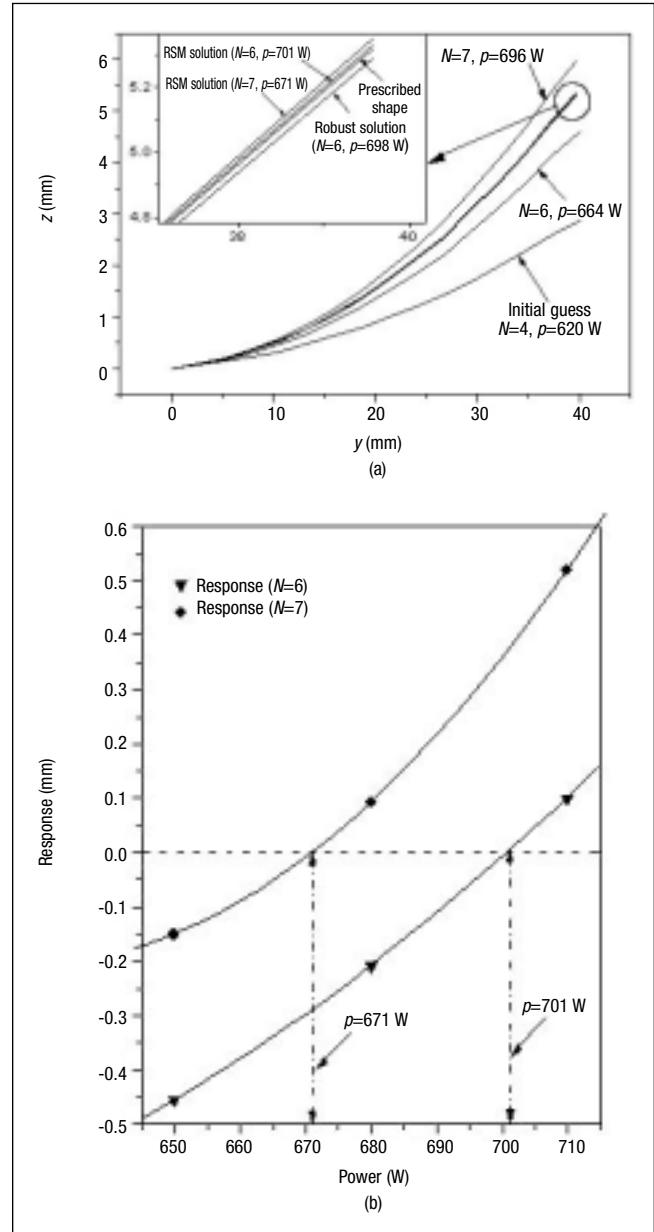developed and discussed in Cases 2-4. As mentioned

Figure 8
Linear Case 1
(a) Design evolution toward the prescribed shape and (b) Responses
near target zero while integer design variable *N*=6 and 7

in section 2, for all experiments and simulation,
laser scanning velocity is kept as $v = 50$ mm/s and
laser beam spot size is kept as $D_b = 4$ mm.

7.1 Linear Case 1

In this case, the square plate is considered, and the
desirable shape (*Figure 8a*) is prescribed in terms of
the following process parameters: number of scan
paths $N = 6$ and laser power $p_i = p = 700$ W. The scan
paths are equally spaced. The way the prescribed
shape is specified is to facilitate comparison of the

design result with the prescription. The task here is to find power p and the number of scan paths N to minimize the difference between the shape formed using the found condition and that using the prescribed condition [Eq. (3)].

Optimal Design

To apply RSM, an initial design point, $N = 4$ and $p = 620$ W, is arbitrarily chosen. The corresponding initial shape is shown in *Figure 8a*. A two-level factorial design is conducted with half width $\Delta N = 1$ and $\Delta p = 30$ W. As outlined in section 5, bending angles under the factorial design conditions are obtained from interpolating the experimental results shown in *Figure 4a*. To mimic the forming process repeatability characteristics, normally distributed random numbers are generated and added to each bending angle value. The standard deviation of the random numbers is chosen as the same as that shown in *Figure 4b* in the form of error bars. These bending angles are used to determine corresponding shapes of the generatrix, and the shapes in turn are used to determine the objective function values h [Eq. (3)]. The objective function values h are the responses in the factorial design.

A first-order regression model is fitted based on the factorial design and the direction of the steepest descent is determined from the coefficients of the regression model. At each movement along the steepest descent direction, the response obtained from the regression model is compared with that based on the experimental result (*Figure 4a*) to examine if this model is still valid. The percentage discrepancies of the comparison at the initial point and at the first movement along the path are 0.42% and 2.22%, respectively, which are considered to indicate that the direction of steepest descent path is valid at these points. The responses h at these points are –1.316 and –0.928, respectively, according to Eq. (3) and the consideration of the sign associated with the equation. After the next movement along the path ($N = 6$ and $p = 664$ W shown in *Figure 8a*), however, the percentage discrepancy increases to 5.87%, which is considered to indicate that the direction is no longer valid at this point. Hence, another two-level factorial design is conducted based on this point and a new steepest descent path is calculated. The new initial point ($N = 6$ and $p = 664$ W) and the next point along the new path ($N = 7$ and $p = 696$ W) have responses $h = -0.5$ and 0.21,

respectively. The change of sign is clearly indicative of "overshooting"; that is, the possible solution shape is bent more than the prescribed shape, which is also shown in *Figure 8a*. This indicates that the optimum condition is in the vicinity of the last movement and normally a three-level factorial design needs to be considered.

In this case, however, the design variable N is subject to integer constraint and the solution must lie on either $N = 6$ or 7. The branch-and-bound approach discussed in section 3 is applied and for this two-variable case it is quite straightforward. As shown in *Figure 8b*, three-level single-factor (p) designs are conducted separately at $N = 6$ and $N = 7$ and quadratic models are fitted for each. The quadratic equation for $N = 6$ is found as

$$h = 3.57 \times 10^{-5}p^2 - 0.0393p + 10.02 \qquad (12)$$

Because the second-order model is fitted with three points, it is an exact fit and thus the residual is zero. Solving the equations for zero response gives optimal solutions $p = 701$ W for $N = 6$ and $p = 671$ W for $N = 7$, as shown in *Figure 8b*. This indicates that multiple solutions are possible. An additional objective function, such as one that minimizes production time, screens out the solution ($p = 671$ W for $N = 7$). The optimization result ($N = 6$ and $p = 701$ W) agrees very well with the prescribed value ($N = 6$ and $p = 700$ W). The optimization process toward the prescribed shape is shown in *Figure 8*, which includes prescribed shape, initial design, some intermediate shapes, and final design.

Robust Design

In practice, the laser power output may fluctuate slightly. To make the design more robust, that is, insensitive to the variation in input variables, propagation of error (POE) is calculated based on Eqs. (6) and (14), and assumed power standard deviation $\sigma_p = 6$W as

$$POE = 4.29 \times 10^{-4}p - 0.236 \qquad (13)$$

Because the residual term in Eq. (12) is zero, thus the residual variance here is also zero. The response h is scaled to a desirability function D_1 ranged from [0,1] according to Eq. (8) because the response problem is of the "target is the best" type, where $T_1 = 0$ (target), L_1 is set as -0.15, and U_1 is set as $+0.15$
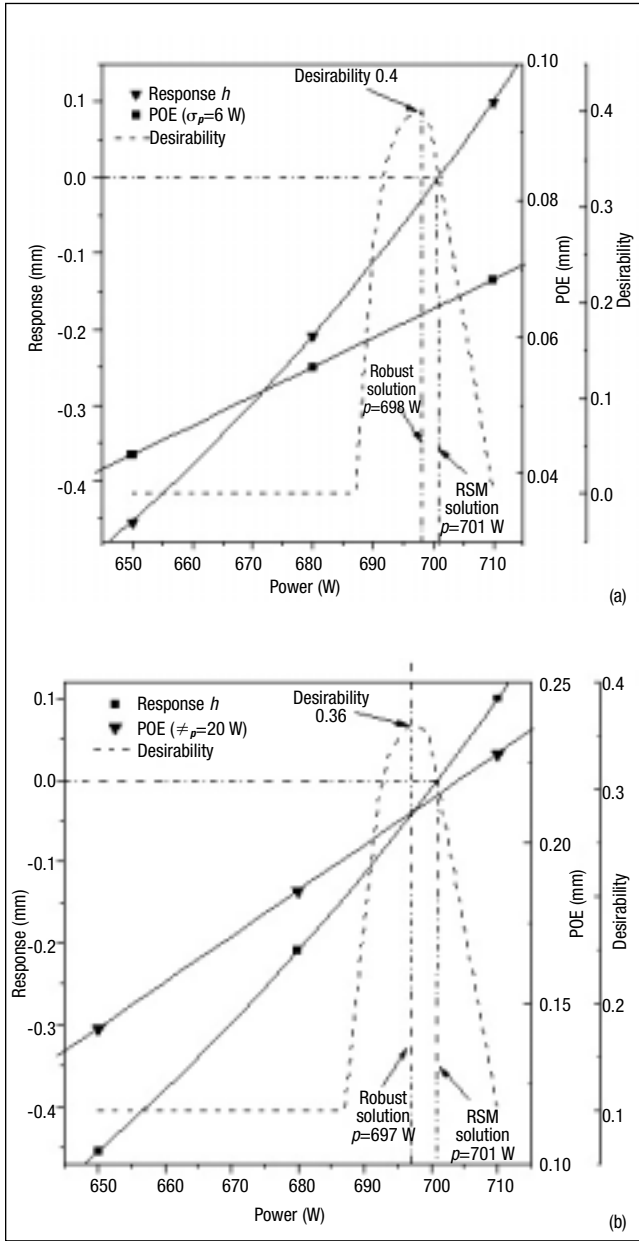
Figure 9
Linear Case 1: Relationship of Response, POE, and Desirability
(a) Standard deviation in laser power σp=6 W and (b) σp=20 W

search, is used to find the variable p that maximizes the overall desirability. The maximum value of desirability, 0.4, is found at $p = 698$ W, where the POE value is lower than that at the optimal solution ($p = 701$ W), and the response value is -0.003. At the optimal solution, the desirability is about 0.33 and the response is obviously zero. The robust design, therefore, balances between the response and POE. Please note the value of overall desirability remains zero until p reaches about 688 W, which is associated with the L_1 value of -0.15. This means that all the solutions smaller than 688 W are not desired because the responses below 688 W are too far away from the desired response of zero. In this case, the robust design does not differ much from the optimal solution, but the design process is generally applicable.

Figure 9b shows the relationship among input variable p with response, POE, and desirability when the standard deviation in laser power σ_p is set as 20 W. As seen, the robust solution moves further away from optimization value 701 W to 696.7 W. However, the maximum value of desirability reduces to 0.36, compared with 0.4 in *Figure 9a*. This indicates that as input variation increases, additional sacrifice on the optimization part has to be made to make the design robust.

7.2 Linear Case 2

In this case, the desired shape is prescribed in terms of a generatrix that is a second-order polyno-

mial $\quad z = 4\left(\dfrac{y}{40}\right)^2 + 2\left(\dfrac{y}{40}\right) \quad$, as seen in *Figure 10*,

and its curvature increases with y. It is obvious that evenly spaced scanning paths are no longer appropriate, that is, $d_{i+1} - d_i \neq d_i - d_{i-1}$, resulting in a large number of design variables and making the RSM-based optimal design less feasible. As seen from *Figure 10*, however, the curvature of the given profile decreases monotonically. Because the trend of spacing between adjacent laser paths is closely related to the curvature of the prescribed shape, the following control function is proposed to relate all d_i's

$$d_i = 40\left(\dfrac{i}{N}\right)^m \tag{14}$$

where d_i specifies the position of the ith laser path, m is the design variable to be determined, and N is

to ensure the robust design is not off the optimal solution too much. The POE is also scaled to a desirability function D_2 according to Eq. (9) because the POE problem is of the "minimization" type, where T_2 is set as 0.042 (for $p = 650$ W) and U_2 is set as 0.068 (for $p = 710$ W) according to Eq. (13). The overall desirability D is then expressed as the geometry mean of D_1 and D_2 using Eq. (7). As seen in *Figure 9a*, the overall desirability function D is a continuous, nonlinear, piecewise function, and therefore a direct search method, downhill simplex
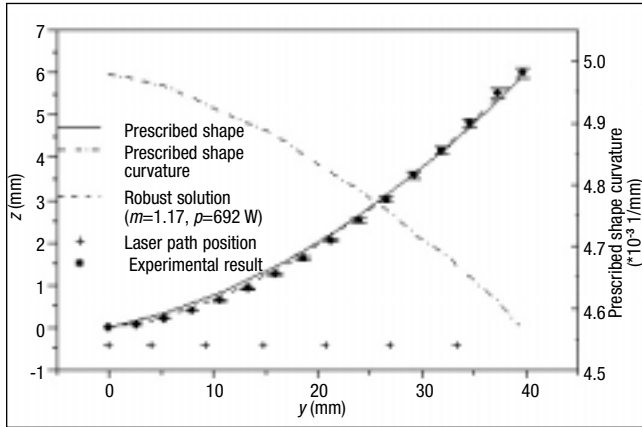
Figure 10
Linear Case 2: Comparison of Robust Solution and Prescribed Shape

the number of laser scan paths. In this case, N is set as 7. The problem, therefore, becomes to determine the value of laser power p and exponent m to achieve the given profile. In an effort to keep the total number of design variables at a manageable level, the power-law expression of Eq. (14) is envisioned to be able to describe the trend that spacing d_i increases with i, according to the desirable shape whose curvature decreases with i. This may lose some generality, but if a large number of design variables is not a concern for DOE, there will be no need to impose Eq. (16), and all d_i's can be treated as independent variables. In this sense, the approach employed is reasonably general.

The same process as in the previous case starts with arbitrarily choosing an initial design at $m = 1.2$ and $p = 650$ W with half width of 0.2 and 30 W, respectively, although there is no need to deal with integer design valuables in this case. The response function is found as

$$h = 1.576 - 5.81m + 0.0073p - 1.13m^2 - 1.14 \times 10^6 p^2 + 0.015mp \quad (15)$$

As seen in *Figure 11a*, all points on the contour of zero response represent optimal solutions. Thus, another objective function, POE, is used to obtain the most desired solution.

Suppose the variations in m and p are 0.02 and 6 W, respectively, the POE is constructed using Eqs. (6) and (17) as

$$POE = \sqrt{\frac{9.38 \times 10^{-8} p^2 - 6.87 \times 10^{-5} p - 3.02 \times 10^{-5}}{mp + 2.29 \times 10^{-3} m + 0.0105 m^2 + 0.02}} \quad (16)$$

in which the residual variance of 0.0725 is included. h and POE are again scaled to desirability functions ranging between [0,1] with h constrained between $[-0.15, 0.15]$. The overall desirability D is then calculated. POE desirability in two-dimensional contour and in three-dimensional form are plotted in *Figure 11b* to *11d*. It is not surprising to observe that the "ridge" of the overall desirability surface somewhat coincides with the zero response contour. As seen from *Figure 11c*, the most desirable value is 0.8013 corresponding to $p = 692$ W and $m = 1.17$. With this m value and Eq. (14), laser path positions, d_i's, are calculated and plotted in the form of crosses in *Figure 10*, along with the final robust solution and prescribed shape. As expected, laser path locations become coarser with decreasing curvature of the prescribed shape. The profile based on the robust solution agrees with the prescribed profile. Note the predictions shown in *Figures 11a* and *11b* represent the response and POE values, respectively, corresponding to the robust solution ($p = 692$ W and $m = 1.17$).

7.3 Circular Case 1

Similar to the first two cases, consecutive laser scans are considered independent from each other. Because the quarter-circle plate is formed by revolving a generatrix around the *z*-axis, the design problem becomes how to achieve a desired generatrix. In this case, the prescribed shape is an arc with radius of 360 mm (i.e., $z = 360 - (360 - r^2)^{0.5}$). The number of concentric scan paths is specified as $N = 8$. The problem is to find the positions of each path, r_i's, and the corresponding laser powers, $p_i = p$. Note that although the curvature of the desired arc is constant, bending angle for a given power varies with radial position, as seen in *Figures 4b* and *4c*. Therefore, r_i's cannot be equally spaced. Furthermore, it is seen from the figures that bending angle does not vary with radial position r monotonically. With the observation and the need to limit the number of design variables, a third-order polynomial function

$$r_i = m\left(\frac{i}{N}\right) + n\left(\frac{i}{N}\right)^2 + o\left(\frac{i}{N}\right)^3 \quad (i = 1, 2, ..., N = 8)$$

is proposed to relate r_i's in this case. Hence, the inverse design problem is reduced to determine power, p, and coefficients, m, n, and o.

The optimal design begins at an arbitrarily chosen initial design point $p = 600$ W, $m = 0.5$, $n = 2$, and
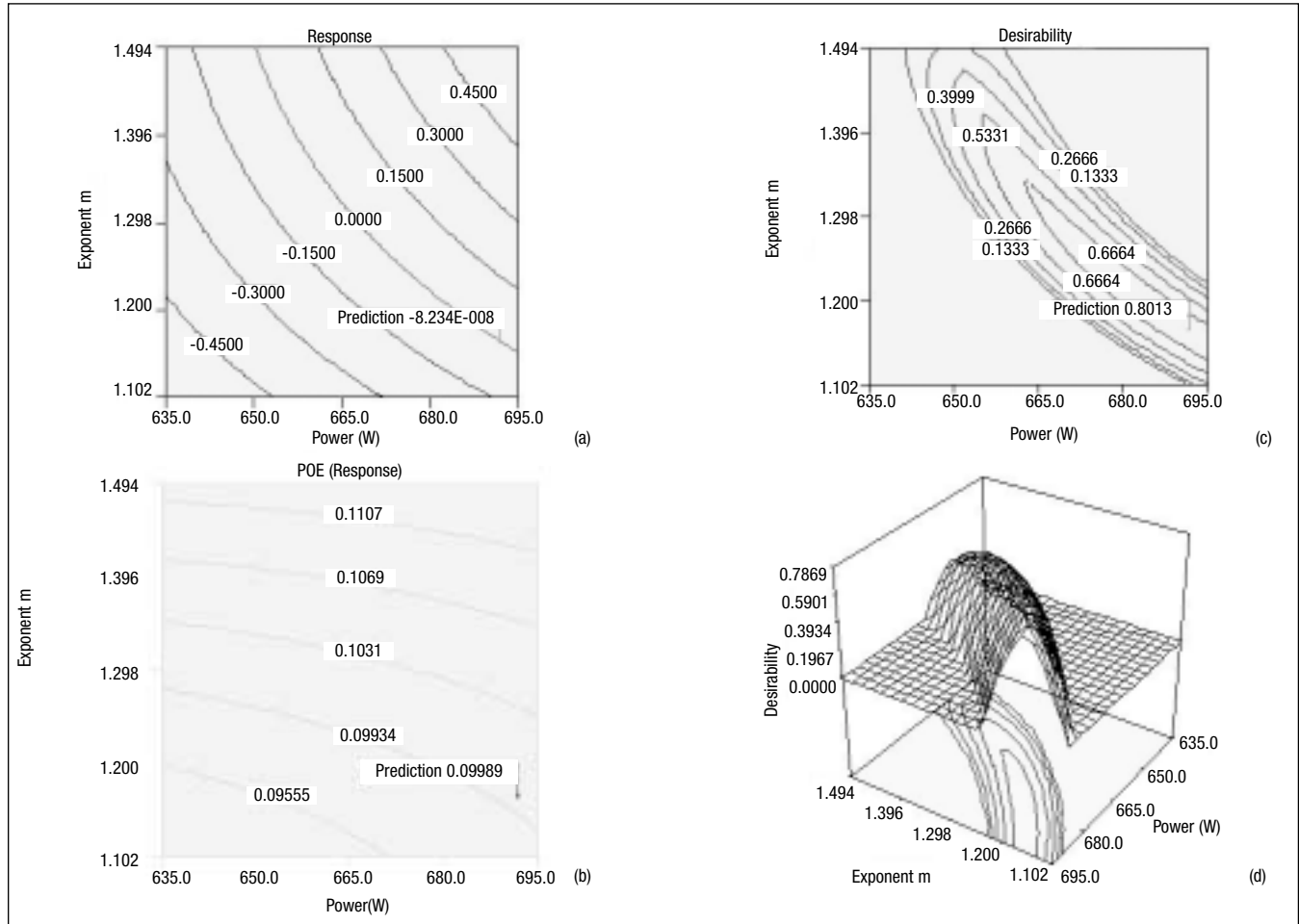
Figure 11
Linear Case 2
(a) Contour plot of response; (b) Contour plot of POE; (c) 2-D contour plot of desirability, the robust design has the highest desirability of 0.8013 for the case; and (d) 3-D plot of desirability ("Predictions" shown in (a) and (b) represent response and POE values corresponding to the robust design).

$o = -1$ with half-width $\Delta p = 20$ W, $\Delta m = 0.1$, $\Delta n = 0.1$, and $\Delta o = 0.1$. The rest is the same as in Linear Case 2. *Figure 12a* shows the prescribed shape and robust designs. The solution shows a good fit with the prescribed shape. The laser path position r_i and spacing between two adjacent paths ($r_i - r_{i-1}$) are plotted in *Figure 12c*. As shown in the plot, ($r_i - r_{i-1}$) increases as the scan path number increases, namely as the radial position of the scan paths increases, and then decreases slightly. The pattern matches that shown in *Figure 4b*. This shows that, although the prescribed shape has a constant curvature, spacing between adjacent scan paths cannot be a constant because the bending angle for a given power changes with the radial position of the paths.

7.4 Circular Case 2

In this case, the prescribed shape is given as $z = 1.2 \times 10^{-4} r^{2.5}$, which has monotonically increasing

curvatures with radial position (*Figure 12b*). The number of scans is defined as $N = 8$. The problem is to find the positions of each path and the corresponding laser power. Similar to the previous case, the distribution of the laser paths is determined by a third order of polynomial function,

$$r_i = m\left(\frac{i}{N}\right) + n\left(\frac{i}{N}\right)^2 + o\left(\frac{i}{N}\right)^3 \quad (i = 1, 2, ..., N = 8).$$

Therefore, the problem again becomes to determine four decision variables, laser power p and coefficients m, n, and o.

The optimal design begins at an arbitrarily chosen initial design point $p = 640$ W, $m = 2$, $n = 2$, and $o = -1$ with half-width $\Delta p = 20$ W, $\Delta m = 0.1$, $\Delta n = 0.1$, and $\Delta o = 0.1$. The rest is the same as in the previous two cases. *Figure 12b* shows the prescribed shape and robust design profile. The laser path positions and spacing between adjacent paths are again plot-
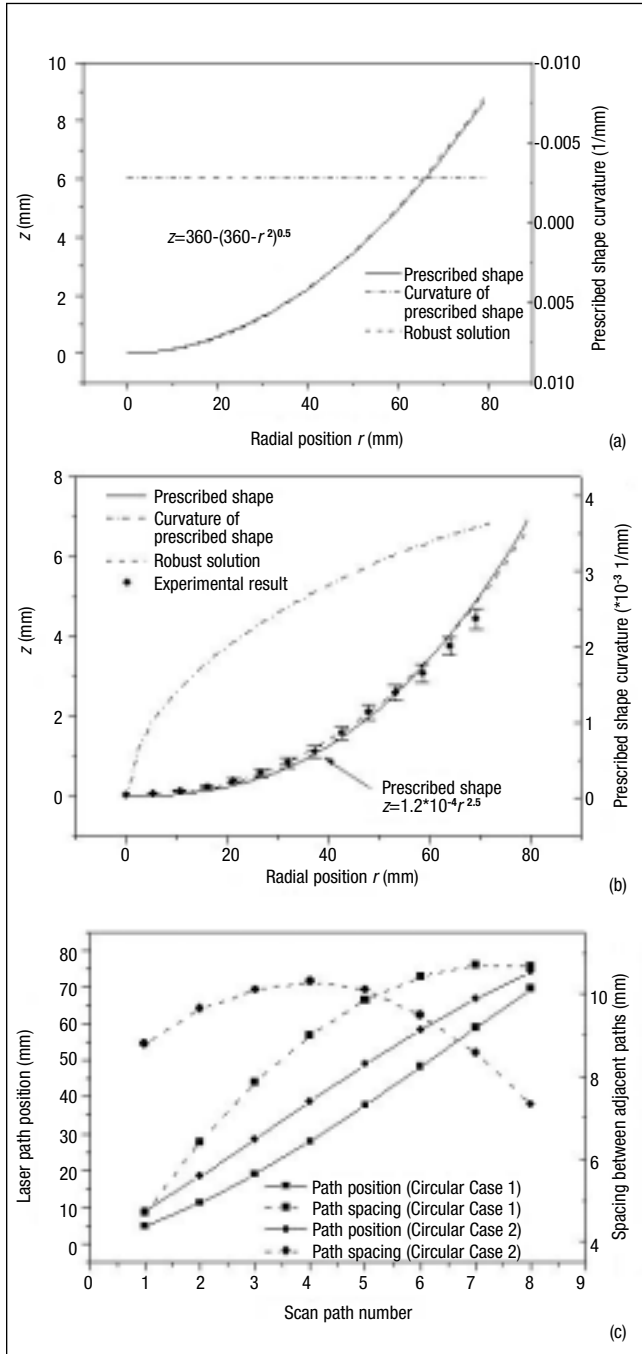
Figure 12
(a) Circular Case 1: prescribed shape with constant curvature; (b) Circular Case 2: prescribed shape with varying curvatures, dots represent experimental results with error bars representing standard deviation of three samples; and (c) Comparison of spacing between adjacent paths for Circular Case 1 and 2

ted in *Figure 12c*. As seen, the spacing between adjacent paths increases and then decreases, but the pattern differs from that in Circular Case 1. This difference can be explained by the difference in curvature of the prescribed shapes. In this case, the curvature of the prescribed shape increases with radial

distance and thus the spacing between adjacent paths needs to become smaller.

Laser forming experiments were conducted under the condition determined by the robust design. As seen in *Figure 12b*, the experimental result shows a good fit at smaller radial positions but some discrepancy at larger radial positions. This is because the errors inevitably introduced during the optimization process (e.g., using summation of bending angles of single scans for multiscanned sheets) get accumulated when the radial position becomes large.

8. Conclusions

It is shown that the proposed optimal and robust design schemes are feasible and effective for the class of shapes considered. Integer design variables are effectively dealt with by using standard methods such as the branch-and-bound method and by integrating with RSM. The hypothesis of independence of scans in multiscan forming is proven valid via experiments and simulation for a certain range of spacing between adjacent scanning paths. This significantly reduces the need for a large number of experiments. To reduce the number of design variables, the laser path positions are specified by polynomials. The adequate order of such polynomials is chosen based on the curvature pattern of the prescribed shapes.

Acknowledgment

References

Bao, J. and Yao, Y.L. (2001). "Analysis and prediction of edge effects in laser bending." *Journal of Mfg. Science and Engg.* (v123), pp53-61.

Boley, B.A. and Weiner, J.H. (1997). *Theory of Thermal Stresses.* Dover Publications, Inc.

Cheng, J. and Yao, Y.L. (2001a). "Cooling effects in multiscan laser forming." *Journal of Manufacturing Processes* (v3, n1), pp60-72.

Cheng, J. and Yao, Y.L. (2001b). "Microstructure integrated modeling of multiscan laser forming." *Proc.* of ICALEO '01.

Derringer, G. and Suich, R. (1980). "Simultaneous optimization of several response variables." *Journal of Quality Technology* (v12), pp214-219.

Hennige, T. (2000). "Development of irradiation strategies for 3D-laser forming." *Journal of Materials Processing Technology* (v103), pp102-108.

Hennige, T.; Holzer, S.; and Vollertsen, F. (1997). "On the working accuracy of laser bending." *Journal of Materials Processing Technology* (v71), pp422-432.

Hsiao, Y.C.; Shimizu, H.; Lee, F.; Maher, W.; and Masubuchi, K. (1997). "Finite element modeling of laser forming." *Proc.* of ICALEO, section A, pp31-39.

Kobayashi, S. (1989). *Metal Forming and the Finite Element Method.* New York: Oxford Univ. Press.

Kraber, S.L. and Whitcomb, P.J. (1996). "Robust design-reducing transmitted variation." 50th Annual Quality Congress, Indianapolis, IN.

Magee, J.; Watkins, K.G.; and Hennige, T. (1999). "Symmetrical laser forming." *Proc.* of ICALEO, section F, pp77-86.

Magee, J.; Watkins, K.G.; and Steen, W.M. (1998). "Advances in laser forming." *Journal of Laser Applications* (v10, n6), pp235-246.

Miller, R.E. (2000). *Optimization Foundations and Applications.* New York: John Wiley & Sons, pp352-360.

Myers, R.H. and Montgomery, D.C. (1995). *Response Surface Methodology.* New York: John Wiley & Sons.

Shimizu, H. (1997). "A heating process algorithm for metal forming by a moving heat source." Master's thesis. Cambridge, MA: Massachusetts Institute of Technology.

Taha, H.A. (1987). *Operations Research.* New York: Macmillan Publishing Co., pp317-322.

Vollertsen, F. (1994). "Mechanisms and models for laser forming." *Proc.* of LANE '94.

Authors' Biographies

Chao Liu is a PhD candidate in mechanical engineering at Columbia University. Y. Lawrence Yao is a professor of mechanical engineering and director of the Manufacturing Research Lab at Columbia University, where his research group works on laser forming, laser shock peening, and laser micromachining. Yao has a PhD from the University of Wisconsin-Madison.